JOURNAL OF COMPUTATIONAL PHYSICS 7, 46–60 (1971)

A Numerical Method for Calculating Transient Creep Flows*

WILLIAM E. PRACHT

University of California, Los Alamos Scientific Laboratory, Los Alamos, New Mexico 87544

Received February 27, 1970

A method is presented for the numerical solution of the transient, low Reynolds number flow of incompressible fluids with free surfaces. The usual numerical stability restrictions related to the viscous diffusion coefficient are avoided by an implicit differencing scheme. The properties of the method are illustrated by several calculational examples.

INTRODUCTION

There exist many fluid flow problems of practical importance in which the viscous forces are dominant. In a few special cases it is possible to obtain analytical solutions, usually by omitting the nonlinear inertia terms from the full Navier–Stokes equations [1]. However, there are many important problems for which it is impossible to obtain an adequate solution.

Several numerical techniques have been developed for the solution of viscous, incompressible flow problems. A few are listed in Refs. [2] and [3]. These methods, however, apply principally to problems for which the inertial forces are larger than the viscous forces, i.e., the Reynolds number ($\equiv LU/\nu$) > 1. Here L and U represent a typical dimension and velocity of the flow, and ν is the kinematic viscosity. Due to limitations related to numerical stability restrictions these methods cannot be efficiently applied to flow problems for which $\mathrm{Re} < 1.0$. This paper describes a technique that has been developed to investigate incompressible flow in this Reynolds number range. It has been developed as an extension to the Marker-and-Cell (MAC) method [3], and is called the MACRL technique. Since the full Navier–Stokes equations are used, MACRL applies equally well to flow problems in the intermediate Reynolds number range. In this way, MACRL extends the applicability of MAC to such slow flows as continental drift, glacier flow, and lubricant flow.

* This work was performed under the auspices of the United States Atomic Energy Commission.

A previous extension of this type by Hung [4] was developed for confined flow calculations. His objective was to achieve complete time centering rather than to extend the technique to low Reynolds numbers. Accordingly he did not require an implicit formulation of the boundary conditions, such as the present technique has been found to require.

The lower limit, $\mathrm{Re} \approx 1$, on the flow Reynolds number for explicit finite-difference techniques is related to the numerical stability requirement

$$\frac{\nu\,\delta t}{\delta x^2} < \frac{1}{4}, \tag{1}$$

where δt is the time step per calculation cycle and δx is the finite-difference cell size. To demonstrate a consequence of this limit, we can rewrite Eq. (1) as

$$(4N)\left(\frac{U\,\delta t}{\delta x}\right) < \mathrm{Re}, \tag{2}$$

where $N = L/\delta x$. Condition (2) can be satisfied for low Reynolds number problems by choosing an appropriately small δt. However, for efficiency, δt should be chosen so that the fluid moves about half a mesh interval per time step, i.e., $U\,\delta t/\delta x \approx 1/2$. Condition (2) can then be expressed as a measure of the smallest Reynolds number that can be efficiently calculated for a given number of cells across a typical dimension of the problem,

$$\mathrm{Re} > 2N. \tag{3}$$

To illustrate how the MACRL technique overcomes this restriction, we may contrast the stability properties of two finite-difference approximations to a simple one-dimensional diffusion equation,

$$\frac{u_j^{n+1} - u_j{}^n}{\delta t} = \frac{\nu}{\delta x^2}\,(u_{j+1}^n - 2u_j{}^n + u_{j-1}^n), \tag{4}$$

$$\frac{u_j^{n+1} - u_j{}^n}{\delta t} = \frac{\nu}{\delta x^2}\,(u_{j+1}^{n+1} - 2u_j^{n+1} + u_{j-1}^{n+1}), \tag{5}$$

where $u_j{}^n$ denotes $u(j\,\delta x, n\,\delta t)$. The equations differ in the time level of the u's on the right sides. Equation (4), which is analogous to the MAC method, employs u's evaluated at cycle number n. In Eq. (5), however, they are time-advanced as in MACRL.

A simple stability analysis shows that the restriction for Eq. (4) is $\nu\,\delta t/\delta x^2 < 1/2$, while Eq. (5) is stable for all values of ν, δt, and δx. To solve the implicit coupled

Navier–Stokes equations analogous to Eq. (5) requires a rather lengthy numerical procedure, but this is mitigated by the larger allowable δt. It is this type of implicit finite-difference approximation to the Navier–Stokes equations that makes practical the solution of low Reynolds number problems.

To incorporate this into the MAC method, however, has required several basic modifications to the technique. The modifications are (1) An implicit finite-difference approximation of the viscous terms in the momentum equations, (2) a revised formulation of the free surface boundary conditions, and (3) a new iterative procedure for solving the equations.

Like MAC, the MACRL method is a finite-difference technique for solving the full, time-dependent Navier–Stokes equations, together with the incompressibility condition. We use these equations in the following form:

$$\frac{\partial \mathbf{u}}{\partial t} = -\nabla \cdot (\mathbf{uu}) - \nabla \phi - \nu \nabla \times (\nabla \times \mathbf{u}) + \mathbf{g}, \tag{6}$$

$$\nabla \cdot \mathbf{u} = 0, \tag{7}$$

where $\mathbf{u}$ is the velocity, $\mathbf{g}$ a body force, and ϕ is the ratio of pressure to constant density. These equations are solved numerically with the aid of a network of fixed rectangular cells. To obtain a solution, the fluid configuration is advanced successively through a series of small time increments δt.

In addition to advancing the set of flow variables each cycle, the coordinates of a set of massless particles are updated. Just as in MAC, these marker particles are initially distributed throughout the fluid and are moved each cycle with the local fluid velocity. These particles aid in flow visualization and serve to keep track of the changing position and orientation of the free surface.

Method of Solution for Confined Flow

From Eq. (6) the following finite-difference approximations can be derived, in which the viscous terms are written in the same manner as Eq. (5),

$$\begin{aligned}\frac{u^{n+1}_{i+1/2,j} - u^{n}_{i+1/2,j}}{\delta t} = {} & \frac{(u^2)^n_{i,j} - (u^2)^n_{i+1,j}}{\delta x} \\ & + \frac{(uv)^n_{i+1/2,j-1/2} - (uv)^n_{i+1/2,j+1/2}}{\delta y} + \frac{(\phi)^{n+1}_{i,j} - (\phi)^{n+1}_{i+1,j}}{\delta x} + g_x \\ & - \frac{\nu}{\delta x\, \delta y}\left[(v)^{n+1}_{i+1,j+1/2} - (v)^{n+1}_{i,j+1/2} - (v)^{n+1}_{i+1,j-1/2} + (v)^{n+1}_{i,j-1/2}\right] \\ & + \frac{\nu}{\delta y^2}\left[(u)^{n+1}_{i+1/2,j+1} + (u)^{n+1}_{i+1/2,j-1} - 2(u)^{n+1}_{i+1/2,j}\right],\end{aligned} \tag{8}$$

$$\frac{(v)^{n+1}_{i,j+1/2} - (v)^{n}_{i,j+1/2}}{\delta t} = \frac{(v^2)^{n}_{i,j} - (v^2)^{n}_{i,j+1}}{\delta y}$$

$$+ \frac{(uv)^{n}_{i-1/2,j+1/2} - (uv)^{n}_{i+1/2,j+1/2}}{\delta x} + \frac{(\phi)^{n+1}_{i,j} - (\phi)^{n+1}_{i,j+1}}{\delta y} + g_v$$

$$+ \frac{\nu}{\delta x^2}\left[(v)^{n+1}_{i+1,j+1/2} + (v)^{n+1}_{i-1,j+1/2} - 2(v)^{n+1}_{i,j+1/2}\right]$$

$$+ \frac{\nu}{\delta x\,\delta y}\left[(u)^{n+1}_{i-1/2,j+1} - (u)^{n+1}_{i-1/2,j} - (u)^{n+1}_{i+1/2,j+1} + (u)^{n+1}_{i+1/2,j}\right]. \tag{9}$$

The corresponding finite-difference expression for $\nabla \cdot \mathbf{u}$ is

$$D^{n}_{i,j} \equiv \frac{(u)^{n}_{i+1/2,j} - (u)^{n}_{i-1/2,j}}{\delta x} + \frac{(v)^{n}_{i,j+1/2} - (v)^{n}_{i,j-1/2}}{\delta y}. \tag{10}$$

The differenced momentum equations (8) and (9) can be combined to give the following equation for the rate of change of D:

$$\frac{D^{n+1}_{i,j} - D^{n}_{i,j}}{\delta t} = \frac{1}{\delta x^2}\left[2(\phi)^{n+1}_{i,j} - (\phi)^{n+1}_{i+1,j} - (\phi)^{n+1}_{i-1,j}\right]$$

$$+ \frac{1}{\delta y^2}\left[2(\phi)^{n+1}_{i,j} - (\phi)^{n+1}_{i,j+1} - (\phi)^{n+1}_{i,j-1}\right] - (Q)^{n}_{i,j}, \tag{11}$$

where

$$Q^{n}_{i,j} \equiv \frac{1}{\delta x^2}\left[(u^2)^{n}_{i+1,j} - 2(u^2)^{n}_{i,j} + (u^2)^{n}_{i-1,j}\right]$$

$$+ \frac{1}{\delta y^2}\left[(v^2)^{n}_{i,j+1} - 2(v^2)^{n}_{i,j} + (v^2)^{n}_{i,j-1}\right] \tag{12}$$

$$+ \frac{2}{\delta x\,\delta y}\left[(uv)^{n}_{i+1/2,j+1/2} - (uv)^{n}_{i-1/2,j+1/2} - (uv)^{n}_{i+1/2,j-1/2} + (uv)^{n}_{i-1/2,j-1/2}\right].$$

The subscripts i and j refer to cell locations, $x = i\,\delta x$, $y = j\,\delta y$, while the superscript n counts time cycles, $t = n\,\delta t$. Cell centers are designated by integer values of i and j; cell edges by half integer values, as $i \pm \frac{1}{2}$ and $j \pm \frac{1}{2}$. Figure 1 illustrates the location of the field variables.

These equations form the basis of the MACRL method. To solve them, we assume that the field variables are available at the beginning of a cycle, either as a result of the previous cycle of calculation or as specified initial conditions. The objective of the solution for each cycle is to obtain a set of pressures that can be inserted into the momentum equations for the calculation of new velocities

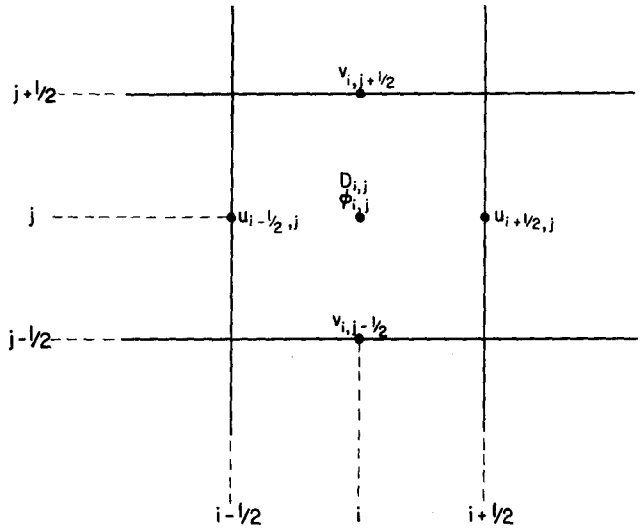

FIG. 1. Field variable placement in a calculation cell.

such that $D_{i,j}^{n+1} = 0$ for every cell. Accordingly, with $D_{i,j}^{n+1} = 0$ in Eq. (11), that equation becomes an implicit expression that can be solved for the pressures. Allowing for slight inaccuracy in the previous cycle solution, the values of $D_{i,j}^{n}$ are, however, retained in Eq. (11), giving the corrective procedure that has been discussed previously [5].

Due to the implicit form of the viscous and pressure terms in Eqs. (8) and (9) and the implicit nature of Poisson's equation, Eq. (11), we have three sets of coupled, simultaneous equations to solve at each time step. This is true despite the apparent completeness of Eq. (11) for the solution of the new-time pressures. The reason for this is that the boundary conditions on ϕ are expressed in terms of derivatives of the velocities, which, for consistent implicit treatment, must be the end-of-cycle velocities. As shown in Eqs. (8) and (9), however, these in turn depend upon the new-time pressures, thereby coupling all of the equations together. To see this specifically, consider the boundary conditions on the pressure for the case of a rigid, no-slip wall on the left side of the computing mesh. The boundary conditions there are that the tangential velocity, v, and the normal velocity, u, vanish at all times. From Eq. (8), this means that (see Fig. 2)

$$v_{i-1,j+1/2} = -v_{i,j+1/2}$$

and

$$\phi_{i,j}^{n+1} - \phi_{i-1,j}^{n+1} + \frac{2\nu}{\delta y}(v_{i,j+1/2}^{n+1} - v_{i,j-1/2}^{n+1}) = 0. \tag{13}$$

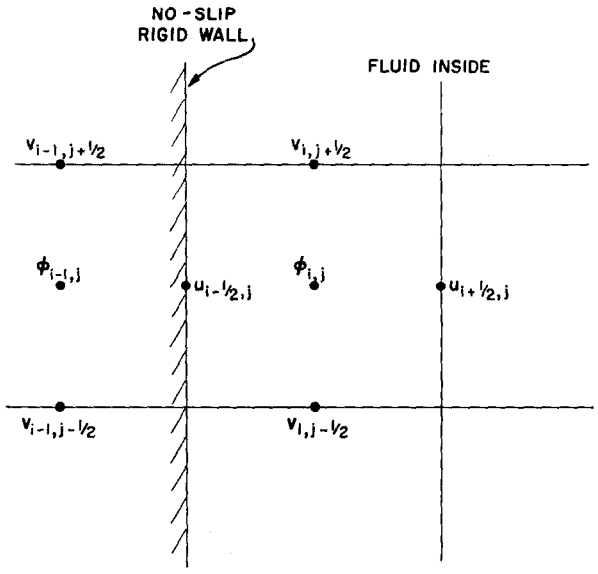

FIG. 2. Variables near a no-slip rigid wall.

If the n-time velocities had been used in Eq. (13), then the pressures and velocity equations would not be coupled together, but numerical experiments with this have shown that such an explicit boundary treatment introduces intolerable numerical instabilities at the walls.

Each calculation time step or cycle is based on the following sequence of events:

(1) The velocities and pressures for each calculational cell are made available either from initial conditions or the preceding cycle. Also the coordinates of the marker particles are available.

(2) The D or discrepancy term, Eq. (10), is calculated from the n-time velocity field. Convection terms and $Q_{i,j}$, Eq. (12), are calculated for use in the iteration that is to follow.

(3) Equations (8), (9), and (11) are solved simultaneously by an iteration technique in such a way that the new-time velocity divergence, $D_{i,j}^{n+1}$, is everywhere zero. This iteration procedure produces the advanced time $(n + 1)$ pressures and velocities for every cell.

(4) All marker particles are moved according to a local average of the velocities nearest each particle.

(5) Necessary bookkeeping chores are performed and output in the form of field variable prints or marker particle configuration plots can be accomplished if desired.

The solution of the set of simultaneous equations required in Step 3 can be accomplished by the use of a Gauss–Seidel or Liebman relaxation procedure. The convergence rate and efficiency of this iterative solution depends upon the form chosen by the user, and would vary considerably with circumstances. The process used in MACRL is to solve these equations for each cell, each iteration. When, for example, we solve these equations for cell (i, j), we first solve Eq. (11), in which $D_{i,j}^{n+1}$ is set to zero, for $\phi_{i,j}$, next Eq. (8) for $u_{i+1/2,j}$, and finally Eq. (9) for $v_{i,j+1/2}$; then advance to cell $(i + 1, j)$ and repeat the process.

It has been found that for problems where $\mathrm{Re} \ll 1$, an additional procedure should be incorporated into each iteration in order to insure continued conservation. This procedure, which is described in detail in Ref. [6], requires the introduction of a potential function and a second iterative process. This can then accomplish accurate conservation with considerable efficiency.

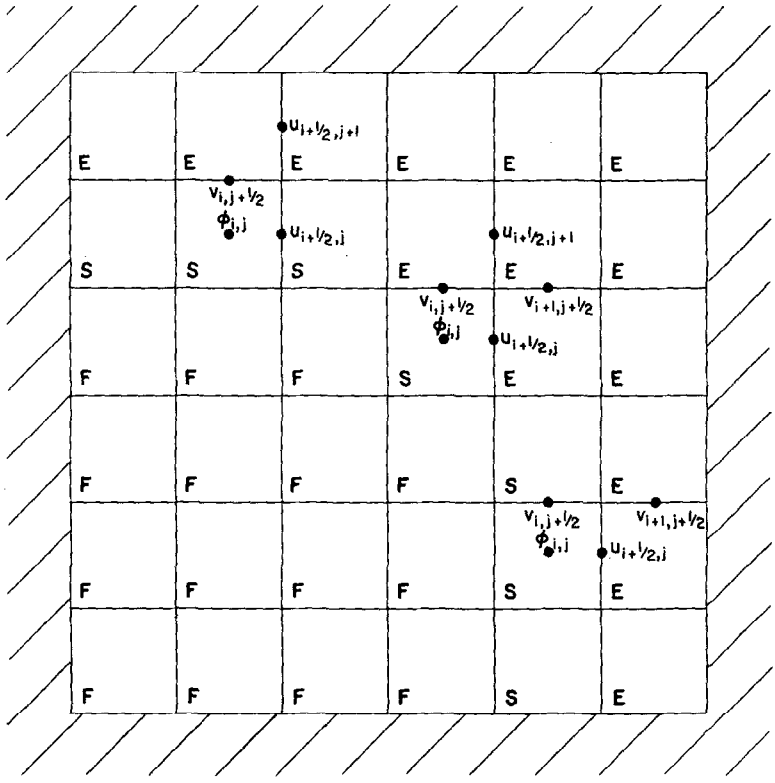

FIG. 3. Sample mesh showing variables needed for three surface cell orientations.

Method of Solution for Flows with Free Surface

The presence of a free surface in incompressible flow problems complicates the solution technique in several ways. First, a means for recording the changing position and orientation of the free surface is necessary in order to impose the boundary conditions properly. This is accomplished in MACRL in the same way as in the MAC technique, i.e., by means of a set of marker particles that move with the local fluid velocity. These particles indicate which Eulerian cells contain the surface. These cells require special treatment.

The second complication is incorporating the free surface boundary conditions in a consistent implicit manner. The conditions to be satisfied are that the normal and tangential stresses at the surface vanish. A more complete discussion of the free surface stress conditions can be found in Ref. [7] so that only the calculation changes made necessary by the implicit solution procedure of MACRL need be discussed here.

Each calculational step consists of the same sequence of events for all full cells as described in the preceding section. The principal difference here is in the equations used for surface cells.

A sample free surface configuration is shown in Fig. 3. A full cell, labeled F, is one that contains fluid but is not adjacent to an empty cell, labeled E. Surface cells are labeled S. The variables to be found in these cells are indicated in the figure for three possible surface cell orientations; top side open to vacuum, right side open to vacuum, or both top and right sides open.

For surface cells which have one side open to vacuum, the normal stress condition can be written

$$\phi_{\text{sur}} = 2\nu \left(\frac{\partial u_n}{\partial n}\right), \tag{14}$$

and the tangential stress condition is

$$\nu \left(\frac{\partial u_n}{\partial m} + \frac{\partial u_m}{\partial n}\right) = 0, \tag{15}$$

where ϕ_{sur} refers to the value of ϕ in the surface cell, n refers to the outward normal direction of the free surface (assumed perpendicular to the open side), and m to the tangential direction.

For the specific case of a surface cell (i, j) having its top side open to an empty cell at $(i, j + \frac{1}{2})$, condition (14) becomes, in implicit finite-difference form,

$$\phi_{i,j}^{n+1} = \frac{2\nu}{\delta y} (v_{i,j+1/2}^{n+1} - v_{i,j-1/2}^{n+1}). \tag{16}$$

Equation (16), Eq. (8), and the condition $D_{i,j} = 0$ can be manipulated into an expression with the unknown v's and ϕ's eliminated. The resulting equation can be solved for the velocity on the right side of the cell, using results from the previous iteration for the unknown quantities on the right. In this case, we write

$$u^{n+1}_{i+1/2,j} = \frac{\delta t}{\xi}\left[uc^n_{i,j} + g_x + \frac{u^n_{i+1/2,j}}{\delta t} + \frac{3\nu}{\delta x^2}\left(u^{n+1}_{i+3/2,j} + u^{n+1}_{i-1/2,j}\right) + \frac{\nu}{\delta y^2}\left(u^{n+1}_{i+1/2,j+1} + u^{n+1}_{i+1/2,j-1}\right)\right], \tag{17}$$

where $\xi \equiv 1 + (6\nu\,\delta t/\delta x^2) + (2\nu\,\delta t/\delta y^2)$ and

$$uc^n_{i,j} = \frac{(u^2)^n_{i,j} - (u^2)^n_{i+1,j}}{\delta x} + \frac{(uv)^n_{i+1/2,j-1/2} - (uv)^n_{i+1/2,j+1/2}}{\delta y}.$$

The velocity at the open side, $v_{i,j+1/2}$, then follows uniquely from the condition $D_{i,j} = 0$. Finally, Eq. (16) is solved for $\phi^{n+1}_{i,j}$. In addition to the velocities on the sides of the surface cell, the calculation requires the velocities of the adjacent empty cell ($u_{i+1/2,j+1}$ in Fig. 3). This can be determined from the finite-difference approximation to the tangential stress condition, Eq. (15),

$$u^{n+1}_{i+1/2,j+1} = \frac{\delta y}{\delta x}\left(v^{n+1}_{i,j+1/2} - v^{n+1}_{i+1,j+1/2}\right) + u^{n+1}_{i+1/2,j}. \tag{18}$$

The equations for a surface cell with its right side open to an empty cell $(i + \frac{1}{2}, j)$ are similarly derived. In this case, the expression for the velocity on the top side of the cell is

$$v^{n+1}_{i,j+1/2} = \frac{\delta t}{\zeta}\left[vc^n_{i,j} + g_y + \frac{v^n_{i,j+1/2}}{\delta t} + \frac{3\nu}{\delta y^2}\left(v^{n+1}_{i,j+3/2} + v^{n+1}_{i,j-1/2}\right) + \frac{\nu}{\delta x^2}\left(v^{n+1}_{i+1,j+1/2} + v^{n+1}_{i-1,j+1/2}\right)\right], \tag{19}$$

where $\zeta \equiv 1 + (6\nu\,\delta t/\delta y^2) + (2\nu\,\delta t/\delta x^2)$ and

$$vc^n_{i,j} = \frac{(v^2)^n_{i,j} - (v^2)^n_{i,j+1}}{\delta y} + \frac{(uv)^n_{i-1/2,j+1/2} - (uv)^n_{i+1/2,j+1/2}}{\delta x}.$$

Again the condition $D_{i,j} = 0$ can be used to determine the velocity at the open side. The normal stress condition is then solved for $\phi^{n+1}_{i,j}$. In finite-difference form it is

$$\phi^{n+1}_{i,j} = \frac{2\nu}{\delta x}\left(u^{n+1}_{i+1/2,j} - u^{n+1}_{i-1/2,j}\right). \tag{20}$$

The velocity of the adjacent empty cell is found from the expression

$$v^{n+1}_{i+1,j+1/2} = \frac{\delta x}{\delta y}\left(u^{n+1}_{i+1/2,j} - u^{n+1}_{i+1/2,j+1}\right) + v^{n+1}_{i,j+1/2}\,.$$

Surface cells with two adjacent sides open to vacuum are treated somewhat differently. For these cases we require that $\partial u/\partial x$ and $\partial v/\partial y$ vanish separately in order to simultaneously satisfy both the tangential stress condition (for a diagonal surface) and the vanishing of $D_{i,j}$. This is accomplished by setting each of the open side velocities equal to the velocity at the opposite side.

In this case we need the velocities of both adjacent empty cells. These are also chosen to satisfy the vanishing tangential stress condition. The u velocity on the right side of the empty cell above is set equal to the u velocity of the left side of that cell. The v velocity at the top side of the empty cell on the right is set equal to the v velocity of the bottom of that cell. The pressure in a cell with two open sides is set equal to zero. Other possible one and two open-sided configurations are treated in a similar fashion.

Surface cells with three sides facing vacuum occur relatively infrequently. For these, the velocity at the open side opposite the fluid is set equal to the velocity at the fluid side; the other two sides are calculated to follow freely the effects of body force and to insure that $D_{i,j} = 0$. Cells with all four sides open are treated to allow for motion due to body forces only.

Sample Applications

A discussion of the results of several calculational examples best illustrates the new features of the MACRL technique. The examples chosen include unsteady two-dimensional flow in a square cavity, and the creeping motion of a highly viscous block of tar.

In the first example, fluid initially at rest in a square cavity is set into circulatory motion within the cavity by a boundary moving in its own plane at the top. The several different calculations are characterized by a Reynolds number, $\mathrm{Re} = LU_{\mathrm{wall}}/\nu$, where L and U_{wall} are the constant length and velocity of the top wall and ν is the kinematic viscosity of the fluid. This type of problem is an appropriate first application of this new technique for several reasons. First, cavity flow has been investigated experimentally and numerically so that useful comparisons can be made in order to test the method. Also, since no fluid enters or leaves the system, and the flow is entirely confined by rigid boundaries, new features of the method can be illustrated with relatively simple boundary conditions.

Calculations of the square cavity problem were performed first for Re = 100 so that comparisons could be made with Donovan's results obtained with an explicit MAC method [8]. In both Donovan's MAC program and MACRL, the full unsteady equations are solved, the principal difference being in the time

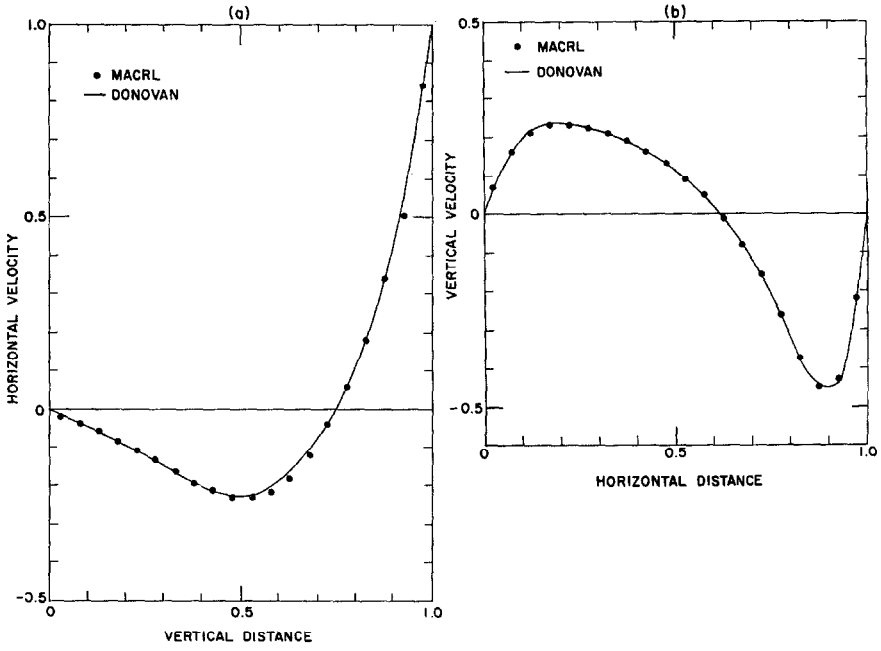

FIG. 4. Graphs showing the calculated velocity (datum points) in comparison with the results of Donovan (solid lines) for (a) horizontal velocity along a vertical traverse through the vortex center, (b) the vertical velocity along a horizontal traverse through the vortex center.

centering of the viscous terms in the finite-difference equations. The two calculations show excellent agreement in the position of the vortex center, and in the patterns of circulation of the marker particles. Another aspect of the agreement is illustrated in Fig. 4a, which shows a late time (steady-state) distribution of x-component velocities along a line perpendicular to the moving surface and passing through the center of the vortex. The distribution of y-component velocity along a line parallel to the moving surface and passing through the vortex center is shown in Fig. 4b.

To illustrate the stability of MACRL under much more stringent circumstances, calculations were run with Re = 1.0 and Re = 0.01 using the same time step as

in the calculation with Re = 100. For the calculation with Re = 0.01, this gave a 6400-fold violation of the explicit stability condition given in Eq. (1).

A comparison of the second and third calculations shows only a slight difference, because in both cases the viscous terms are strongly dominant. Figure 5 shows the steady-state velocity vector configuration for Re = 0.01. Horizontal velocity profiles along a vertical line through the vortex center are shown in Fig. 6, which

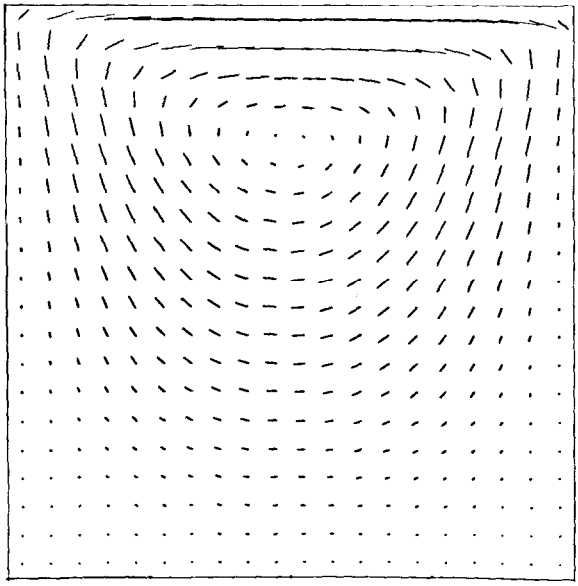

FIG. 5. Steady-state velocity configuration for Re = 0.01, in the square cavity problem.

compares the MACRL solution to the full unsteady equations for Re = 1.0 with the results from the steady equations for Re = 0 by Kawaguti [9] and Burggraf [10].

The large time step used for the Re = 0.01 problem was chosen primarily to demonstrate the stability of the method. To accurately represent the first few cycles of the eddy formation would require an extremely small time step. It can be shown, however, that as the calculation proceeds, the time step could be increased each cycle by a factor proportional to the cycle number. In this way, the calculation could efficiently reach the steady solution and at the same time resolve accurately the early phases of eddy formation.

As a second type of example to exhibit new capabilities of MACRL we calculated the slow flow of a fluid having free surface. The example illustrated in Fig. 7

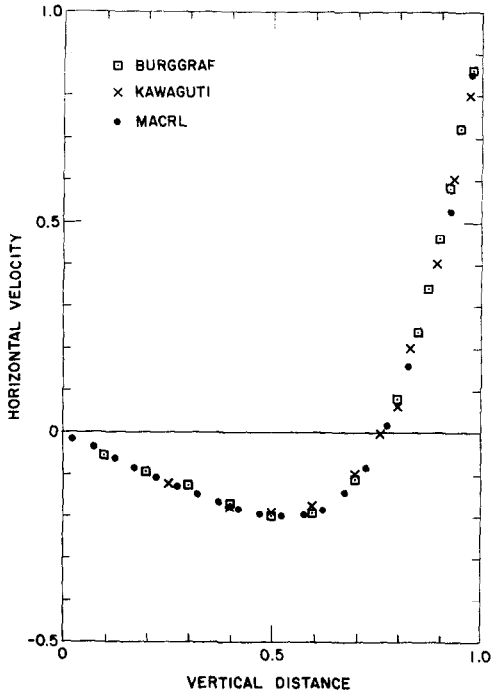

FIG. 6. Graph showing comparison of velocity profiles among MACRL at Re = 1.0, Kawaguti at Re = 0.0, Burggraf at Re = 0.0 for the horizontal velocity along a vertical traverse through the vortex center.

represents the highly viscous slumping motion that would occur if a rectangular block of tar or pitch were placed on a nonslip surface and left undisturbed. Shown here is a sequence of marker particle configurations obtained directly from the calculation. A thin empty layer next to the bottom boundary can be seen in the last two plots. This is a result of the coarse resolution. Since the layer is less than one cell thick, each calculational cell in the layer is treated as though it were full of fluid.

In this, as in all incompressible flow calculations, volume or mass conservation is necessary for accurate results. A conservation check of the tar block problem reveals that $D_{i,j}$ remains negligible for each cell, and the total volume remains

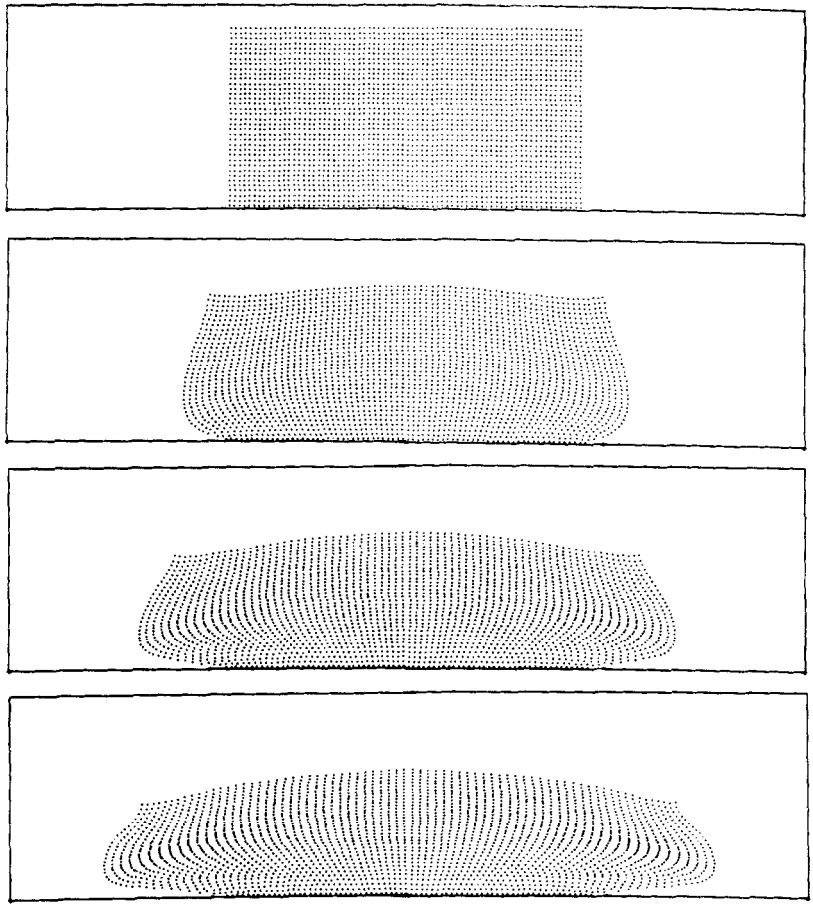

FIG. 7. Fluid configurations representing the slow flow of tar block.

constant throughout the run to within the accuracy that can be measured from the particle configuration plots.

All the calculations discussed in this section were done on a CDC 6600 computer. The results shown in Fig. 5 and Fig. 7 were processed from the computer by the Stromberg Carlson 4020 Microfilm Recorder and were not retouched or altered in any way.

ACKNOWLEDGMENT

The author wishes to express his appreciation to Francis H. Harlow for his many valuable suggestions.

REFERENCES

1. H. SCHLICHTING, "Boundary-Layer Theory," 6th ed., p. 104, McGraw-Hill, New York, 1968.
2. C. W. HIRT, J. L. COOK, AND T. D. BUTLER, *J. Comp. Phys.* **5** (1970), 103–124; J. E. FROMM AND F. H. HARLOW, *Phys. Fluids* **6** (1963), 975; F. H. HARLOW, "Numerical Methods for Fluid Dynamics, an Annotated Bibliography," Los Alamos Scientific Laboratory Report No. LA-4281, 1969.
3. F. H. HARLOW AND J. E. WELCH, *Phys. Fluids* **8** (1965), 2182.
4. T. K. HUNG, Proceedings of Fifth International Congress on Rheology, Kyoto, Japan, 1968.
5. C. W. HIRT AND F. H. HARLOW, *J. Comp. Phys.* **2** (1967), 114.
6. W. E. PRACHT, Proceedings of Second International Conference on Numerical Methods, Berkeley, 1970, to be published.
7. C. W. HIRT AND J. P. SHANNON, *J. Comp. Phys.* **2** (1968), 403.
8. L. F. DONOVAN, *AIAA J.* **8** (1970), 524.
9. M. KAWAGUTI, *J. Phys. Soc. Japan* **16** (1961), 2307.
10. O. R. BURGGRAF, *J. Fluid Mech.* **24** (1966), 113.